Numerical and Experimental Study of Quasi-Static Loading of Aluminum Closed-Cell Foams Using Weaire–Phelan and Kelvin Tessellations

Shakibanezhad, R.; Sadighi, M.; Hedayati, R.

DOI
10.1007/s11242-021-01729-5

Publication date
2022

Document Version
Final published version

Published in
Transport in Porous Media

Transport in Porous Media
https://doi.org/10.1007/s11242-021-01729-5

Numerical and Experimental Study of Quasi-Static Loading of Aluminum Closed-Cell Foams Using Weaire–Phelan and Kelvin Tessellations

R. Shakibanezhad[1] · M. Sadighi[1] · R. Hedayati[2]

Received: 12 February 2021 / Accepted: 15 November 2021

Abstract
Study of porous materials, in particular closed-cell foams, has always attracted researchers' interest due to the advantages these materials offer in applications where low weight, buoyancy, insulation, or energy absorption is of importance. In this study, quasi-static compressive experimental tests are conducted for low-, medium-, and high-density aluminum foams and their mechanical properties are obtained. In addition, two types of lattice structures based on regular repeating unit cells (Kelvin and Weaire–Phelan) are modelled and their suitability for predicting the mechanical behavior of closed-cell foams in quasi-static configuration is evaluated and compared. Due to the irregular structure of cast foams, it is computationally very expensive to reproduce numerical models with similar structural topology. Using tessellation method can be a step forward in investigating various parameters affecting the properties of closed-cell foams. The results indicated that as compared to Kelvin models, the Weaire–Phelan models better mimic the deformation of manufactured specimens. On the contrary, as compared to the Weaire–Phelan models, the mechanical properties obtained from the Kelvin models are in general closer to the experimental results. The study results also showed that as the foam density increases, the densification strain decreases, while all other mechanical properties (elastic modulus, yield stress, plateau stress, and energy absorption capacity) increase.

Keywords Cellular materials · Kelvin · Weaire–Phelan · Quasi-static tests · Numerical modelling · Lattice structure

✉ M. Sadighi
mojtaba@aut.ac.ir

[1] Department of Mechanical Engineering, Amirkabir University of Technology (Tehran Polytechnic), Hafez Ave, Tehran, Iran

[2] Department of Aerospace Structures and Materials, Faculty of Aerospace Engineering, Delft University of Technology (TU Delft), Kluyverweg 1, 2629 HS Delft, The Netherlands

Published online: 20 January 2022

1 Introduction

Study of porous materials, especially closed-cell foams, has always attracted researchers' interest due to the advantages these materials offer in applications where low weight, buoyancy, insulation, or energy absorption is a necessity (Hedayati et al. 2019). Different research areas related to closed-cell foams such as mechanical properties (Jang et al. 2015; Hall et al. 2000; Ramamurty and Paul 2004; Ulbin et al. 2020, 2019; Duarte et al. 2016; Novak et al. 2019; Zhu et al. 2018), heat transfer characteristics (Hu et al. 2020; Baillis and Coquard 2008; Pabst et al. 2018; Baillis et al. 2017; Glicksman and Torpey 1989), manufacturing methods (Tzeng and Ma 2006; Banhart 2001), production process control (Movahedi et al. 2014), and heat/acoustic insulation performance (Glicksman and Lanciani 1991; Opiela et al. 2021;) have been investigated thoroughly in the last decades. Even tough experimental studies (Hall et al. 2000; Ramamurty and Paul 2004; Ulbin et al. 2019; Hedayati and Sadighi 2018; Hedayati et al. 2018a) are the most essential and reliable type of research in this field, interest in computational modeling (Ulbin et al. 2020; Rajendran et al. 2009; Liu et al. 2017) has been continuously increasing in the last decade due to high cost of manufacturing and mechanical testing of foam specimens for experimental tests which limits the material and geometrical parameters that can be investigated systematically.

Many experimental studies have been performed to obtain the properties of closed cell foams (Han et al. 1998; Li et al. 2020; Motz and Pippan 2001; Zenkert and Burman 2009; Andrews et al. 2001; Gibson and Ashby 1999). Andrews et al. (2001) found that elastic modulus and compressive strength of foam enhance by increasing the ratio of specimen size to cell size. Moreover, they concluded that if the number of cells is greater than eight and five for open- and closed-cell foams, respectively, the cell size effect becomes negligible. The influence of other variables such as hollow size, cell dimensions, cell thickness, and anisotropy have been investigated thoroughly by Gibson and Ashby (Gibson and Ashby 1999). Not only experimental tests are expensive to perform, evaluating all the parameters affecting the foam properties in a systematic way is not an easy task. That is why many researchers have approached computational methods in this regard.

Researchers have made many efforts to create a mathematical model capable of predicting the mechanical behavior of foams (Ulbin et al. 2020; Vengatachalam et al. 2019; Koloushani et al. 2018; Abdullahi et al. 2019; Grenestedt and Bassinet 2000; Czekanski et al. 2005; Kadkhodapour and Raeisi 2014; Roberts and Garboczi 2001; Fang et al. 2015; Chen et al. 2017). Such computational models have been based on CT images (Koloushani et al. 2018; Mohammadi Nasrabadi et al. 2016), Voronoi formula (Baillis et al. 2017; Shi et al. 2018; Wang et al. 2017), regular unit cells (Kader et al. 2020a), and macro-mechanical material models (Hedayati and Sadighi 2016; Diebels and Geringer 2014).

Macro-mechanical model is the most popular method as it does not require modelling the micro-structural features of the foam. In this method, the macro-geometry of the foam is modelled and then an appropriate material model capable of mimicking foam behavior is assigned to the foam geometry. However, this modelling technique has the big drawback of not giving the opportunity of investigating the effect of micro-structural features on the foam's overall behavior. This method is, therefore, usually beneficial for multi-component complex structures (Hedayati and Ziaei-Rad 2011; Torkestani et al. 2015), in which the mechanical behavior of the foam is already well-established and in which the complexity of the model does not allow for modelling the foam in detail.

X-ray and CT scan image scanning have given valuable insights into the behavior of structures with complex micro-geometries, including closed-cell foams. The advantage of models obtained from CT images is that they are capable of accurately reconstructing the relatively irregular geometry (pore's distribution, size, and orientation) of the foam. Such studies help to understand the main mechanisms dominating the foam behavior during damage. In other words, observing the cell's internal changes during collapse shows what failure mechanisms have the most contributions in the damage. The results of a study by Kader et al. 2020b have shown that the regions with large void fractions predominantly undergo collapse and subsequently reduce the structural heterogeneity. In another study, it was shown that foams with larger spatial variation of porosity and larger pore concentrations disintegrate earlier (Ulbin et al. 2018). Sun et al. studied uniaxial compression behavior of polymer and aluminum closed-cell foams using experimental tests and X-ray based numerical models. A "zero-yield-stress" response and then a sharp increase in unloading modulus was observed. They claimed that unloading elastic modulus varies during the compression process, and suggested that it would be better to obtain elastic modulus by extrapolating the measured unloading modulus to zero strain (Sun et al. 2016). Despite many advantages they offer, models based on CT images have the drawbacks of being expensive to obtain and high computational cost.

Voronoi tessellation method has been introduced as a numerical measure to reduce computational costs. In Voronoi tessellation method, a large number of points are randomly seeded in 3D space, and then a region is assigned to each point. Afterwards, several walls are constructed automatically around each seed point to separate neighboring regions from each other. Zhu et al. 2018 developed irregular closed-cell foam models based on Voronoi description and using Hill's computational approach to investigate the elastic properties of the structure. The results of homogenized models were compared with the experimental and tomography reconstructed model results, and acceptable agreement was achieved. In another research by Li et al. 2014 based on Voronoi closed-cell foam model, it was found that by increasing the shape irregularity, the stress–strain diagram's plateau region first increases and then decreases. In another study (Shi et al. 2018) based on Voronoi tessellation, it was found out that the initial peak stress and plateau stress are proportional to relative density and loading velocity. Also, the elastic modulus is reduced by increasing the regularity of Voronoi foam. The drawback of Voronoi-based models is that mathematical procedures of implementing the Voronoi technique makes the method relatively complex and time-consuming. Hence, researchers have implemented tessellation of regular unit cells to model behavior of foams (Hedayati et al. 2018b, 2019; Santosa and Wierzbicki 1998; Simone and Gibson 1998).

In tessellation method, a representative volume element (RVE), also known as unit cell, is repeated regularly in 3D space in three main directions to create a lattice structure. Santosa and Wierzbicki 1998 proposed a cubical closed-cell unit cell containing pyramidal corners. Their finite element (FE) model was capable of incorporating fracture predictions in closed-cell foam. Simone and Gibson (Simone and Gibson 1998) proposed a model based on curved cell plates which was able to accurately predict elastic modulus and peak stress. Many unit cell geometries such as cubic-spherical (Nammi et al. 2010), cruciform-pyramidal (Nammi et al. 2010), spherical (Hasan 2010), cruciform-shaped (Hasan 2010), tetrakaidecahedron (Li et al. 2020; Liu and Zhang 2013; Wang et al. 2015), Kelvin (Mills et al. 2009; Giorgi et al. 2010), and Weaire–Phelan (Chen et al. 2017; Buffel et al. 2014) have been proposed and studied to model closed-cell foams. Among all the unit cells, the Kelvin and Weaire–Phelan unit cells have the advantage of creating cells with minimal external surface area when dividing the space (Weaire and Phelan 1994; Thomson 1887).

Minimal external surface area is a crucial parameter when foams are formed which suggests that Kelvin and Weaire–Phelan geometries can model the geometry and thus the behavior of foams the best. Mills et al. (Mills et al. 2009) simulated a model of layers' interaction using Kelvin foam and with consideration of the cells' internal gas pressure. Ghazi et al. (Ghazi et al. 2019) proposed a method to generate closed-cell metallic foam geometry based on microstructural morphological features. In their model, the structural deformations were categorized into three main modes of buckling, bending, and plastic hinge formation. Furthermore, they observed that before the formation of plastic zones, cell walls experience elastic buckling first. In another research, Marvi-Mashhadi et al. developed models based on X-rays from foam structure and studies the effects of cell size, cell distribution, and mass fraction on struts and walls (Marvi-Mashhadi et al. 2018a, 2018b). They proposed an analytical model to predict the effect of internal gas pressure on foam's mechanical behavior (Marvi-Mashhadi et al. 2020). Moreover, Giorgi et al. (Giorgi et al. 2010) modeled aluminum foam using three Kelvin unit cell types with curved, ellipsoidal, and flat walls.

To the best of our knowledge, no work has been dedicated to both numerical and experimental studies of closed-cell foams and to comparison of capability of two basic unit cell shapes (Kelvin and Weaire–Phelan) in predicting the quasi-static behavior of closed-cell foams. Unlike the previous studies where implicit FE modeling has failed to properly predict the post-elastic behavior of the foams due to large deformations and convergence deficiency, we propose a novel numerical model based on explicit formulation. In this study, quasi-static compressive experimental tests are conducted for low-, medium-, and high-density aluminum foams, and their mechanical properties are obtained. Two types of FE models based on regular unit cells (Kelvin and Weaire–Phelan) are constructed, and their suitability for predicting the mechanical behavior of closed-cell foams in static configuration is also evaluated.

2 Materials and Methods

2.1 Experiments

The aluminum foams were manufactured using casting process consisting of three main stages: thickening, foaming, and cooling. The aluminum was first heated up to 600 °C; to prevent the bubbles from floating, calcium was mixed with molten aluminum for 6 min to stabilize the bubbles in the molten aluminum and to increase its viscosity. Afterwards, TiH_2 particles were added to the melted aluminum. Due to heat, the TiH_2 particles were decomposed into hydrogen gas and titanium. The appearance of hydrogen gas in the melted aluminum created bubbles trying to escape the melt. After a suitable foamy structure was formed, the temperature of the system was reduced using blower and cold water to transform the liquid-state bubbles into solid-state bubbles, which in turn, created metallic foam. The density of the foam block varied in the foaming direction due to the hydrogen motion during the manufacturing process. A smooth decreasing density occurred through foaming direction that affected wall thickness. Therefore, the block was divided into three categories of the low, medium, and high density, to investigate the density effect on the mechanical properties.

In previous studies, several cutting processes, such as electrical discharge machining (EDM), band saw (BS), water jet (WJ) cutting, and laser cutting methods (Meng et al.

2019; Liu et al. 2018), have been implemented to cut foam structures. Metallurgical and morphological (Zhu et al. 2018; Yilbas et al. 2014, 2013, 2015) observations have revealed that cutting process affects porous material's mechanical properties significantly. Various processing and machining parameters such as deformation depth, feed rate, spindle speed (Razboršek et al. 2019) in incremental forming and frictional rolling method as well as laser power, scanning speed, gas pressure, cutting forces, and cutting temperatures (Liu et al. 2020) in laser cutting techniques have been previously investigated thoroughly. For instance, Heidari and Yan used single-crystal diamond tools for cutting, and realized that the presence of pores affects the accuracy of cutting mechanism directly (Heidari and Yan 2018). Hangai et al. found out that incorporating NaCl into milling process leads to less fracture in the cell walls (Hangai et al. 2017). Liu et al. proposed a direct laser cutting process to preserve pore structures from damaging and to make efficient regular shapes (Liu et al. 2018).

To prepare the experimental test specimens, first, cooled initial mold was cut to form a rectangular block. Afterwards, the foam bulk was cut into smaller specimens using laser cutting process. Aluminum foams were cut into cubes with dimensions of 40 mm × 40 mm × 40 mm. Special attention was paid to the foaming direction during the experimental tests (Fig. 1) to take into account the direction in which the foam wall thickness and thus foam density decreased. Different densities of the specimens were documented by measuring the dimensions and weights. The specimens were divided into three main categories of density: low (0.2–0.3 gr/cm^3), medium (0.3–0.5 gr/cm^3), and high (> 0.5 gr/cm^3). For each category, three specimens were tested. The compressive tests were performed under constant displacement rate using an STM-50 mechanical test bench. The outputs were obtained as reaction force–displacement curves which were then transformed into stress–strain domain. The tests were continued until the stress began to rise sharply. The compression device and the placement of the specimens are shown in Fig. 2.

In general, under compression, the stress–strain curve obtained from cellular structures is composed of three main regimes (Hedayati and Sadighi 2018; Karaji et al. 2017): first, the elastic regime in which the stress rises sharply in a linear fashion until the first collapses and ruptures start occurring in the cellular structure. After the elastic regime, the second regime, known as plateau regime, starts in which the stress increases very slightly despite the sharp increase in the strain extent. In the final regime, also known as densification regime, the cell walls of the cellular structure come into contact

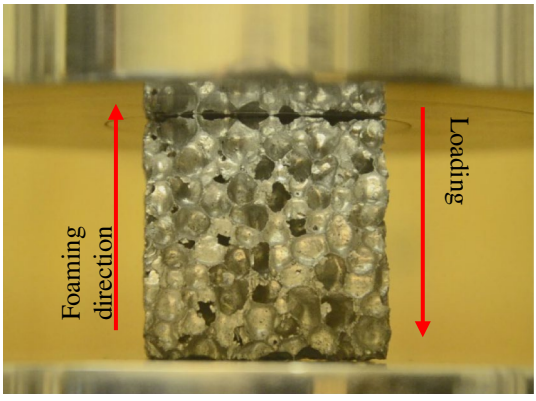

Fig. 1 Foaming and loading directions

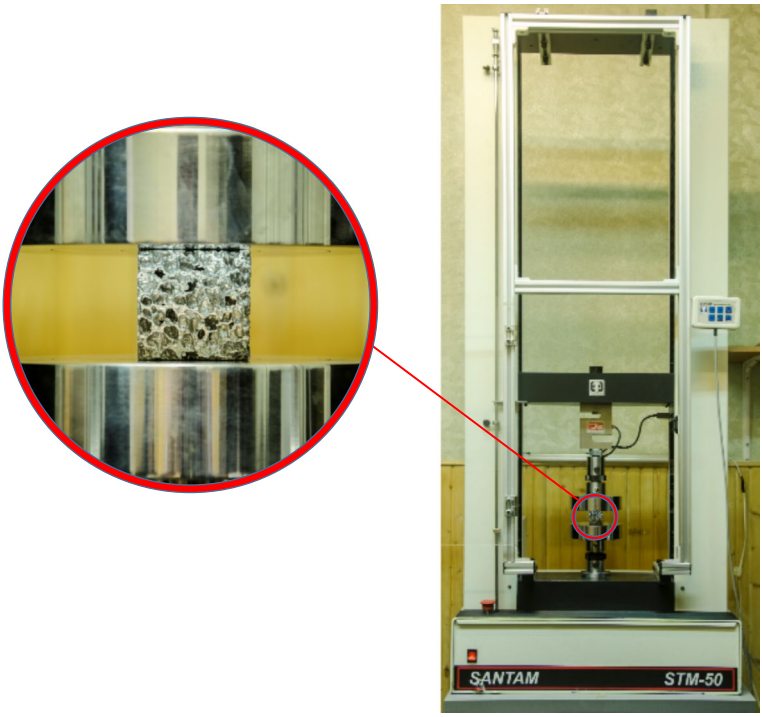

Fig. 2 Compression test device SATNAM STM-50

with one another which leads to an exponential increase in the stress level as more and more walls come into contact with each other.

Using the stress–strain curves, the following mechanical properties were calculated: elastic modulus, yield stress, plateau stress, densification strain, and energy absorption. The ISO standard 13,314:2011 (ISO Standard, 2011) was used to calculate the plateau stress. The arithmetical average of stresses at 0.2 and 0.4 strains was considered as the plateau stress. The elastic modulus was calculated by obtaining the slope of the line connecting the stress–strain curve at 0.2 and 0.7 of the plateau stress. The yield stress was obtained by finding the intersection of a line parallel to the initial linear section of the stress–strain curve and shifted to the right side for 0.2% strain on the one hand and the stress–strain curve itself on the other hand. The densification strain was obtained at the intersection point of lines best fitted to the stress–strain curve in the plateau and densification regimes. The energy absorption was obtained by calculating the area under the stress–strain diagram. The energy absorption was obtained for two cases: up to densification strain and up to maximum applied stress which differed for each density.

2.2 Numerical Modeling

CATIA (Dassault Systèmes, France) and SolidWorks (Dassault Systèmes, France) software packages were used for constructing the geometry of the lattice structures by stacking unit cells. Two types of unit cells, Kelvin and Weaire–Phelan, were considered for numerical simulation. A Kelvin unit cell consists of six square faces and eight

hexagonal faces. A Weaire–Phelan unit cell consists of eight individual cells of two types: two irregular dodecahedron cells which is composed of twelve pentagonal faces, and six tetrakaidecahedron cells which is composed of two hexagonal faces and twelve pentagonal faces. The resulting unit cells were duplicated in three main directions without leaving any space between their faces. After each lattice structure (based on Kelvin or Weaire–Phelan unit cells) was constructed by sufficiently duplicating unit cells in the three main directions (with at least 5 unit cells in each direction, as suggested by Andrews et al. (2001)), it was cut into cubes with specific dimensions to create lattice

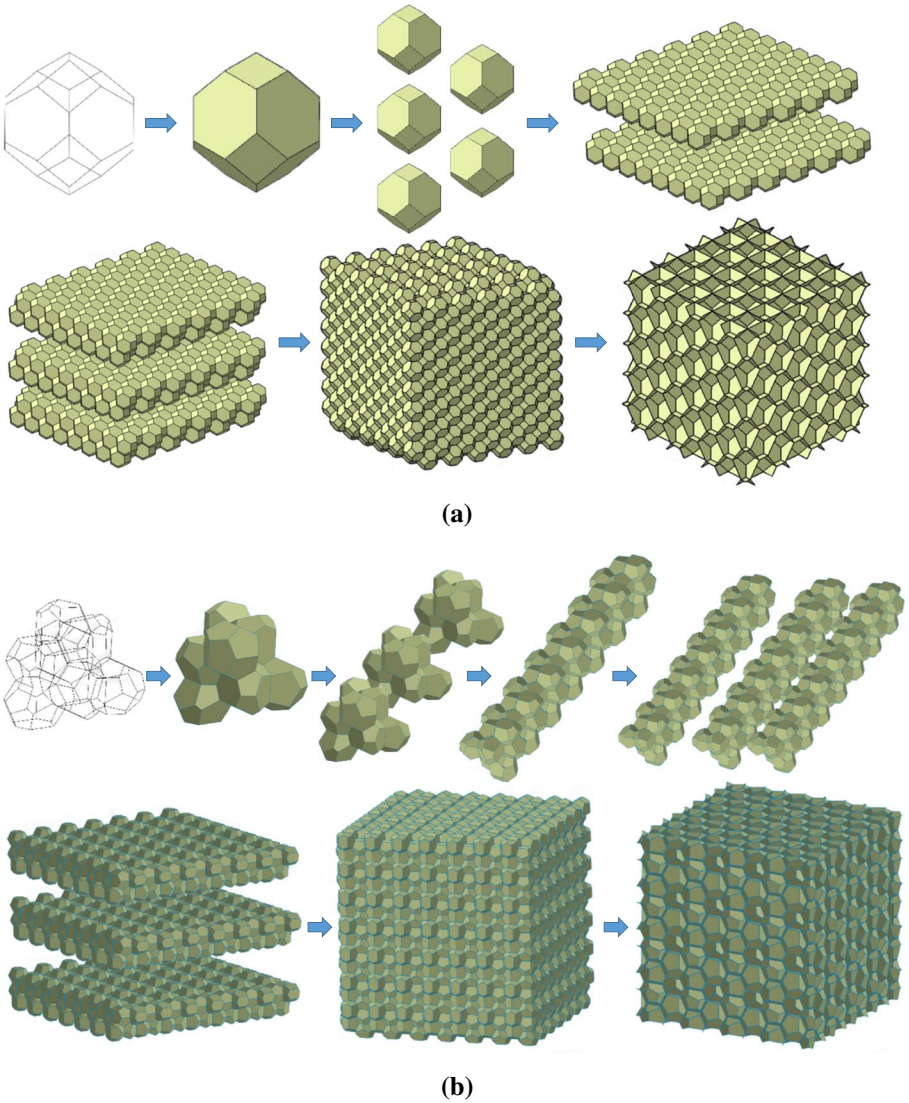

Fig. 3 Construction of lattice structures based on **a** Kelvin and **b** Weaire–Phelan unit cells in the CAD program

Table 1 Utilized density (in gr/cm^3) for different density and model types in numerical modelling

	Low density	Medium density	High density
Kelvin FE model	0.24	0.34	0.53
Weaire–Phelan FE model	0.24	0.34	0.53

structures with smooth external surfaces (Fig. 3). Faces of the unit cells were discretized using shell elements. The densities assigned to different FE models are listed in Table 1.

Abaqus/Explicit was implemented for simulating the quasi-static compression loading process. Boundary conditions representing the actual conditions in the experimental tests were imposed on the top and bottom surfaces. Rigid plates were placed at the top and bottom sides of each lattice structure. The top and the bottom surfaces, as well as all the cell walls should be capable of recognizing each other when they collide in order to contribute to accumulation of stress in the whole lattice structure during the compressive loading. Therefore, general contact type which can take into account the interactions between all exterior faces, analytical rigid surfaces, and shell perimeter edges, was applied to the entire model. Triangular FE elements were used to discretize the models due to their complex geometries at the faces. A mesh sensitivity analysis was performed and element size in the range of 0.5 mm to 0.8 mm was found to be suitable for the simulations. The modeling process in Abaqus for both the Kelvin and Weaire–Phelan lattice structures is demonstrated in Fig. 4.

The aluminum alloy physical and mechanical properties (mass density = 2700 kg/m^3, elastic modulus = 70 GPa, Poisson's ratio = 0.33) were assigned to the model for the simulations. The elastic–plastic stress–strain curves data obtained from experimental

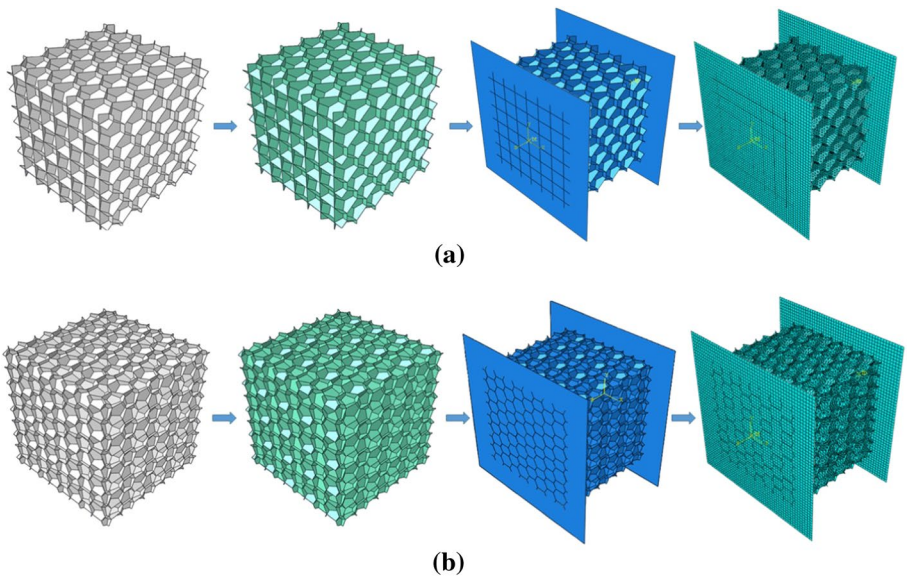

Fig. 4 Importing, assigning mechanical properties, assembling the top and bottom plates, and discretization of **a** Kelvin and **b** Weaire–Phelan foam models in Abaqus

tensile tests on the constituent material (the aluminum alloy) were also assigned to the model.

3 Results and Discussions

Since the foaming direction was considered in the orientation of the specimens placed inside the test rig (the lower density sides of all the foam specimens were always placed on the top side), collapse started from the topmost layer of all the specimens. The collapsing continued sequentially from the topmost cellular layer to the adjacent underneath layers one by one. The plateau region of all the specimens started in the strain range of 0.025 and 0.05.

The stress–strain curves of the low-, medium-, and high-density foams are shown in Fig. 5. The experimental results presented in the stress–strain curves for each density are the average curves obtained for three specimens. The diagrams demonstrate that for high-density specimens, the stress level in the plateau region increases gradually by increasing the strain, whereas for the medium-density foam, the stress in the plateau region remains almost at the same level. As for the low-density foam, the stress level decreases towards the end of the plateau region. In the high-density foams, the particles detached from the specimen during the collapse filled in the hollow spaces inside some cells which led to gradual increase in the stress level in the plateau region. The effect of this phenomenon decreases as the thickness of the walls decreases. In the low-density foams, the particles separated from the foam did not fill the cells at any stage and, therefore, they did not contribute to load bearing of the specimens.

Some repetitive fluctuations occured in the plateau region of the foams as shown in Figs. 5 and 6a. The visual status of the foam specimen at the peaks and troughs of the stress–strain curve is demonstrated in Fig. 6b. Comparing Fig. 6b(iii) and b(iv) suggests noting two critical points. The stress–strain diagram of the specimen has troughs at strains of 0.43 and 0.58, while it has a peak at the strain of 0.47. First, after the

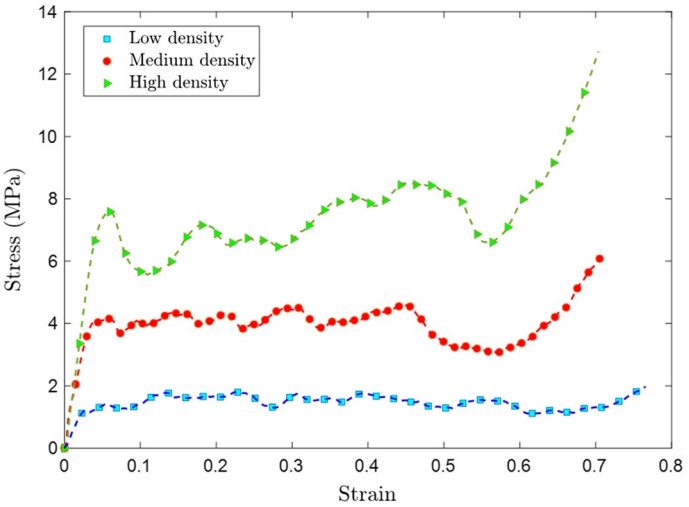

Fig. 5 Stress–strain diagram of compression tests for low-, medium-, and high-density foams

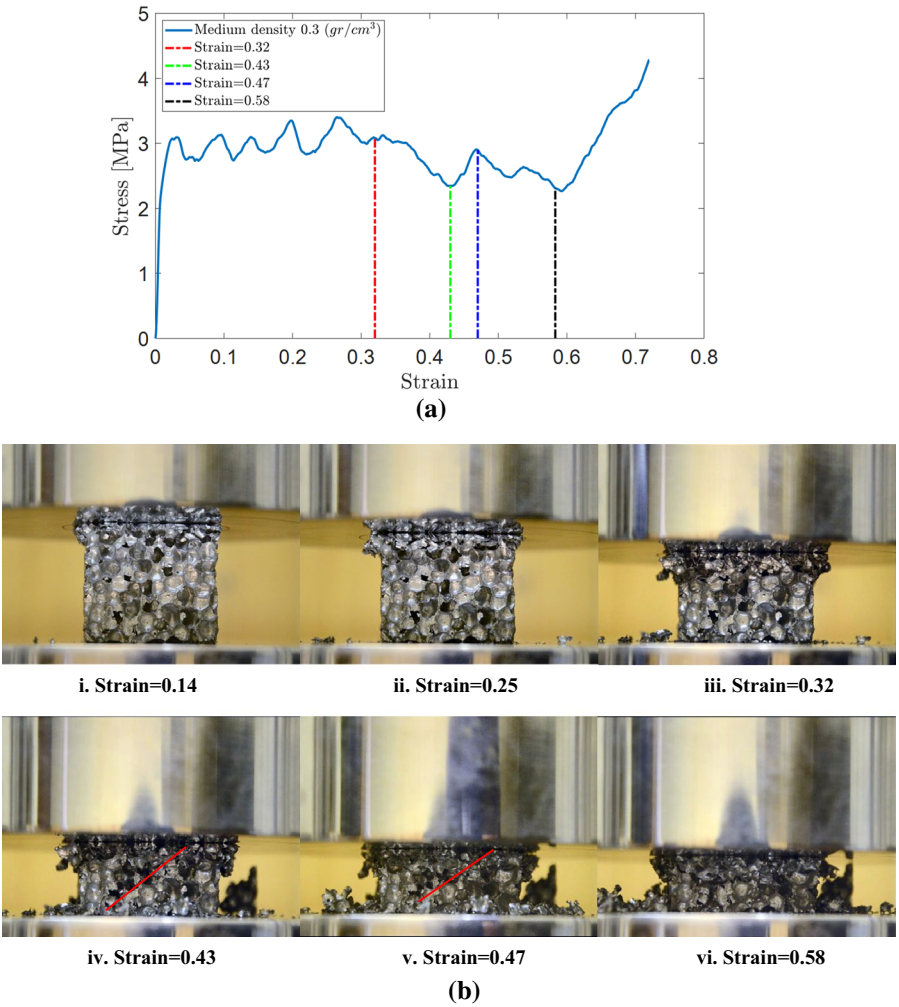

Fig. 6 **a** Stress–strain diagram and **b** deformation of the medium-density specimen. The photographs of specimen in (**b**) is taken at the peaks or troughs of the stress–strain curve of the same specimen shown in (**a**), i.e. at strains of 0.14, 0.25, 0.32, 0.43, 0.47, and 0.58. The red lines mark the fracture planes of the specimen

deformation of the specimen at the strain of 0.32, several fractured and deformed parts are still contributing to load bearing of the specimen. However, at the strain of 0.43, several pieces are detached from the specimen which reduces the load-bearing capacity of the foam specimen. In addition to several relatively small particles, one large detached particle fallen on the lower grip at the strain of 0.43 can be seen in Fig. 6b(iv). Second, a noticeable fracture plane appears at strains higher than 0.32 which is marked on the deformed foam specimen at the strains of 0.43 and 0.47 (Fig. 6b(iv) and b(v)). Appearance of fracture plane as well as detachment of several particles create a trough

in the stress–strain curve of the specimen at the strain of 0.43 (see Fig. 6a). After that, the particles filling the pores lead to an increase in the stress level. The noted process of fracture and detachment of small and large segments (leading to decrease in stress value) and filling of the inner part of the foam by smaller particles (leading to increase in stress value) is repeated several times causing fluctuations in the stress level in the plateau region.

The experimental and numerical stress–strain curves for all foam densities are depicted in Fig. 7. Similar to the experimental compression test results, the stress–strain curves of the numerical simulations also consist of three distinct regimes: linear elastic, plateau, and densification.

As shown in Fig. 7a, for low-density foams, there was good agreement in the linear elastic region between both the Kelvin and Weaire–Phelan models on the one hand and the experimental results on the other hand. In the plateau and densification regimes, the overlapping between the three curves was observed as well. The stress level of the plateau region in the low-density foams started at 1.28–1.48 MPa stress range and it increased to 1.87–2.47 MPa in the end of plateau region. The densification strains for the experimental test, Kelvin FE model, and Weaire–Phelan FE model were 0.76, 0.80, and 0.81 respectively, with a maximum of 6.2% error.

As for the medium-density case (Fig. 7b), similar to the low-density case, the FE models and the experimental tests showed good agreement in the linear elastic and plateau regions. The densification strain started at 0.67, 0.71, and 0.73 for the experimental test, the Kelvin model, and the Weaire–Phelan model, respectively (maximum 8.2% error). The plateau region started at 2.81–3.45 MPa range, and it increased to 4.43–4.88 MPa at the densification point. The difference between the densification strains was more significant in this case as compared to the low-density foam.

Similarly, for high-density foam, the experimental and numerical results showed good agreement in the linear elastic and plateau regions (Fig. 7c). For this type of foam, the difference between numerical and experimental densification strains is greater than the two other foam types. The densification strains of the experimental test, Kelvin model, and Weaire–Phelan model are 0.59, 0.68, and 0.70 with a maximum of 15.7% error. The other difference between the high-density foam and two other foam types was that the plateau region for the high-density foam was not horizontal, and it had an upward slope, starting from 6.18 to 6.75 MPa range and reaching to 13.44–15.13 MPa range at the densification threshold. Moreover, generally, the stress levels in this type of foam was significantly higher than that in two other foam types.

Different foam properties such as elastic modulus, yield stress, plateau stress, densification strain, energy absorption (up to densification point) and energy absorption (including all the three regions) were obtained and are plotted for different density categories in Fig. 8. As for the low-density case, the elastic modulus (Fig. 8a) of the experimental tests ($E = 55.47$ MPa) and numerical results had relatively good agreement with one another (maximally 36.4% error). However, by increase in the density, the difference between the numerical and experimental results decreased, and for high-density foam ($E = 285.6$ MPa), this difference reached its minimum (10.8% maximum error).

A similar trend was observed for the yield stress (Fig. 8b). The maximum difference between the numerical and experimental results occurred in the medium density case (22.2%). Moreover, by increasing the density, the level of yield stress increased and reached its maximum ($\sigma_y = 6.49$ MPa) at high-density. The maximum discrepancies observed between the Kelvin and the Weaire–Phelan model results were 23.6%, 2.8%, and 0.8% for the low-, medium-, and high-density, respectively.

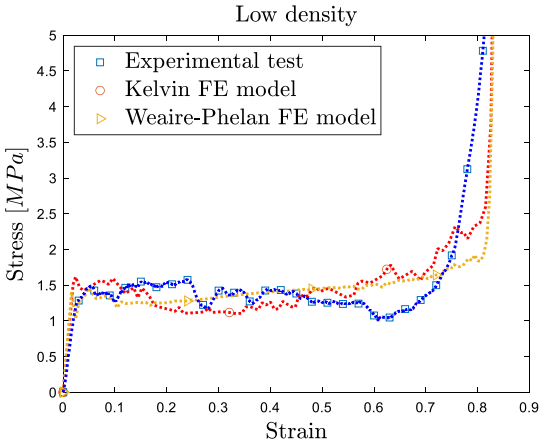

(a)

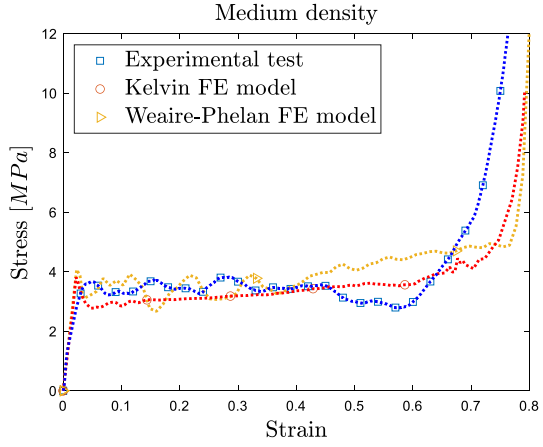

(b)

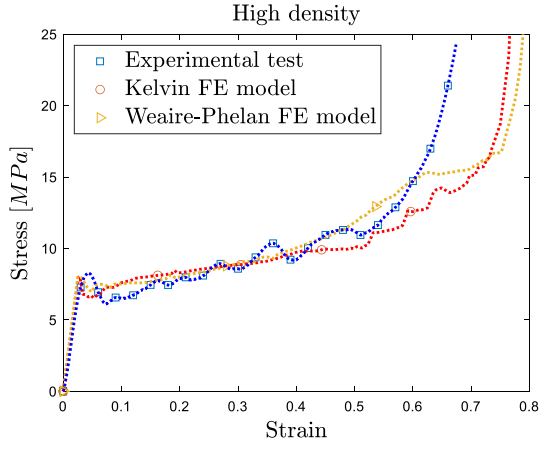

(c)

Fig. 7 Stress–strain diagram of the manufactured foam specimens, Kelvin FE models, and Weaire–Phelan FE models for **a** low density, **b** medium-density, and **c** high-density foams

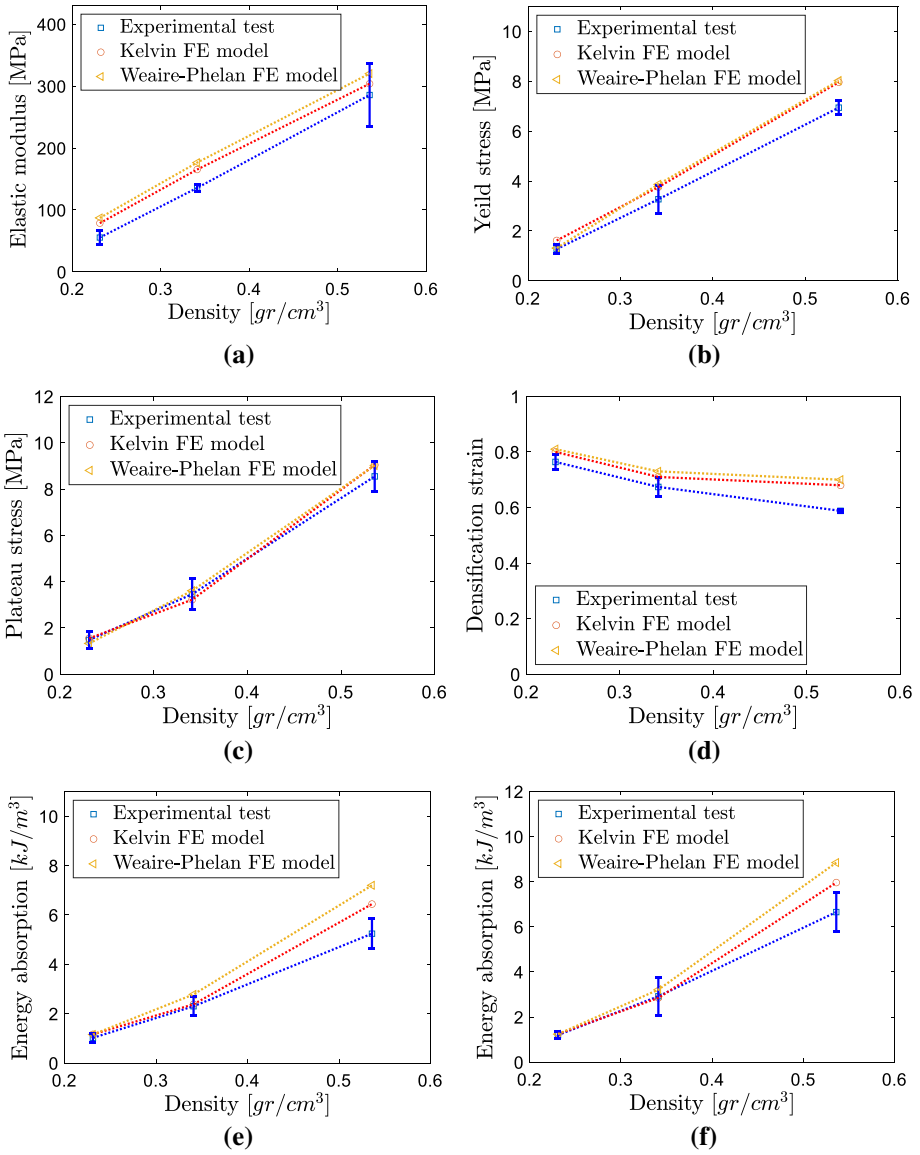

Fig. 8 Variations of mechanical properties of the foam structures with respect to density: **a** Elastic modulus, **b** Yield stress, **c** Plateau stress, **d** Densification strain, **e** Energy absorption (strain = 0 to densification strain), **f** Energy absorption (strain = 0 to end point of the test)

The experimental plateau stress (Fig. 8c) was calculated as 1.48 MPa, 3.45 MPa, and 8.54 MPa for the low-, medium-, and high-density foams, respectively. Moreover, the maximum numerical/experimental difference was 10.1%, 7.1%, and 5.5% for the low-, medium-, and high-density foams, respectively. The plateau stress vs density curve showed an exponential behavior.

Unlike the three above-mentioned mechanical properties (Fig. 8a-c), the densification strain decreased by increasing the foam density (Fig. 8d). The measured densification strains at low density were 0.76, 0.80, and 0.81, respectively, for the foam specimen, the Kelvin model, and the Weaire–Phelan model. By increasing the density, the densification strain slightly decreased to 0.59, 0.68, and 0.70 for, respectively, the foam specimen, the Kelvin model, and the Weaire–Phelan model at the high density.

The amount of energy absorption was calculated up to two different points: (i) from the start of loading till densification threshold, and (ii) from the start of loading up to 5, 12, and 23 MPa stress levels for the low-, medium-, and high-density foams, respectively. As for the case of loading up to the densification strain (Fig. 8e), the energy absorption capacity was 1.02 kJ/m^3, 2.30 kJ/m^3, and 5.24 kJ/m^3 for the low-, medium-, and high-density foams, respectively. The Kelvin and Weaire–Phelan FE models had relatively close energy absorption capacities to each other, but with a maximum difference of 27.2% with respect to experimental results. As for the energy absorption capacity for the whole stress–strain diagrams (Fig. 8f), the experimental values were 1.20 kJ/m^3, 2.92 kJ/m^3, and 6.65 kJ/m^3 for the low-, medium-, and high-density foams. The maximum numerical/experimental discrepancies changed to 1.6%, 9%, and 23.1% for the low-, medium-, and high-density foams, respectively. All the plots presented in Fig. 8 demonstrate that the Kelvin FE model can reproduce the experimental values slightly better than how the Weaire–Phelan does.

The deformation of the foam specimen, the Kelvin model, and the Weaire–Phelan model under compression are visually compared to each other in Fig. 9 at strains of 0, 0.32, 0.43,

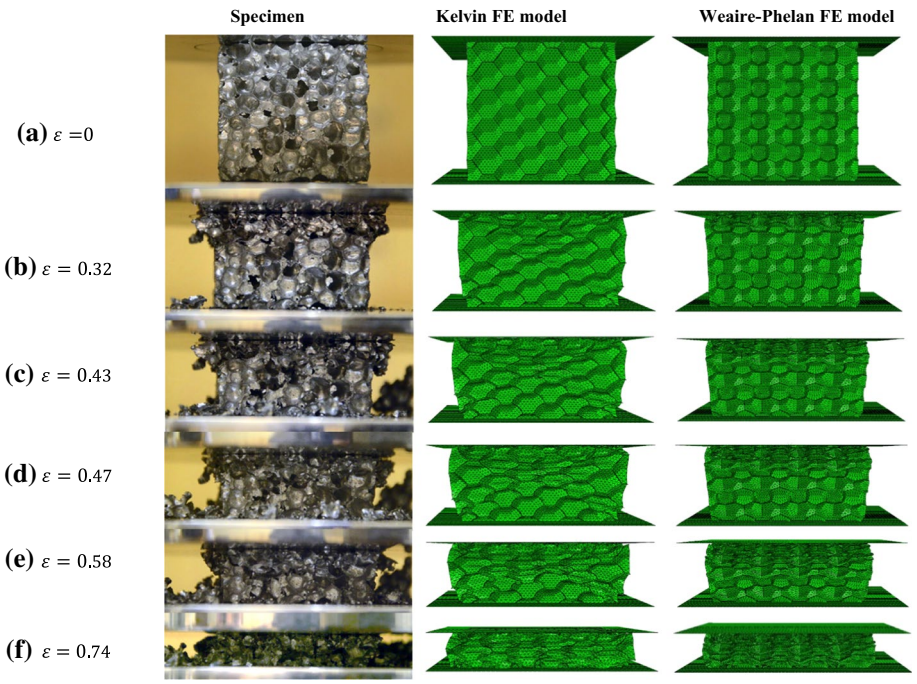

Fig. 9 Deformation of the medium-density foam specimen (left), Kelvin FE model (middle), and Weaire–Phelan FE model (right) at different strain levels: **a** ε = 0, **b** ε = 0.32, **c** ε = 0.43, **d** ε = 0.47, **e** ε = 0.58, and **f** ε = 0.74

0.47, 0.58, and 0.74. A good agreement was observed between the deformation shapes of experimental specimens and the numerical models (Fig. 9a,b). By looking at the cells from micro-structural point of view, it was seen that in the numerical models, at the global strain of 0.32 and 0.58, buckling occurred in the cell walls (mostly pronounced at top half of the foam), and that the cells lost their primary shape. Similar to the experimental test, collapse started from the topmost layer in FE models, and the collapsing continued sequentially from the topmost cellular layer to the adjacent underneath layers one by one. In addition, at the strain of 0.74, the FE models' cell walls came into contact with each other which resulted in observation of densification in the stress–strain model in all the cases. Comparing the Kelvin and Weaire–Phelan FE models demonstrates that the Weaire–Phelan model is more resistant to lateral expansion of the whole model, and therefore, it better mimics the deformation of the actual manufactured specimens (Fig. 9). However, as compared to the Weaire–Phelan model, the mechanical properties obtained from the Kelvin model are in general slightly closer to the experimental results (Fig. 8).

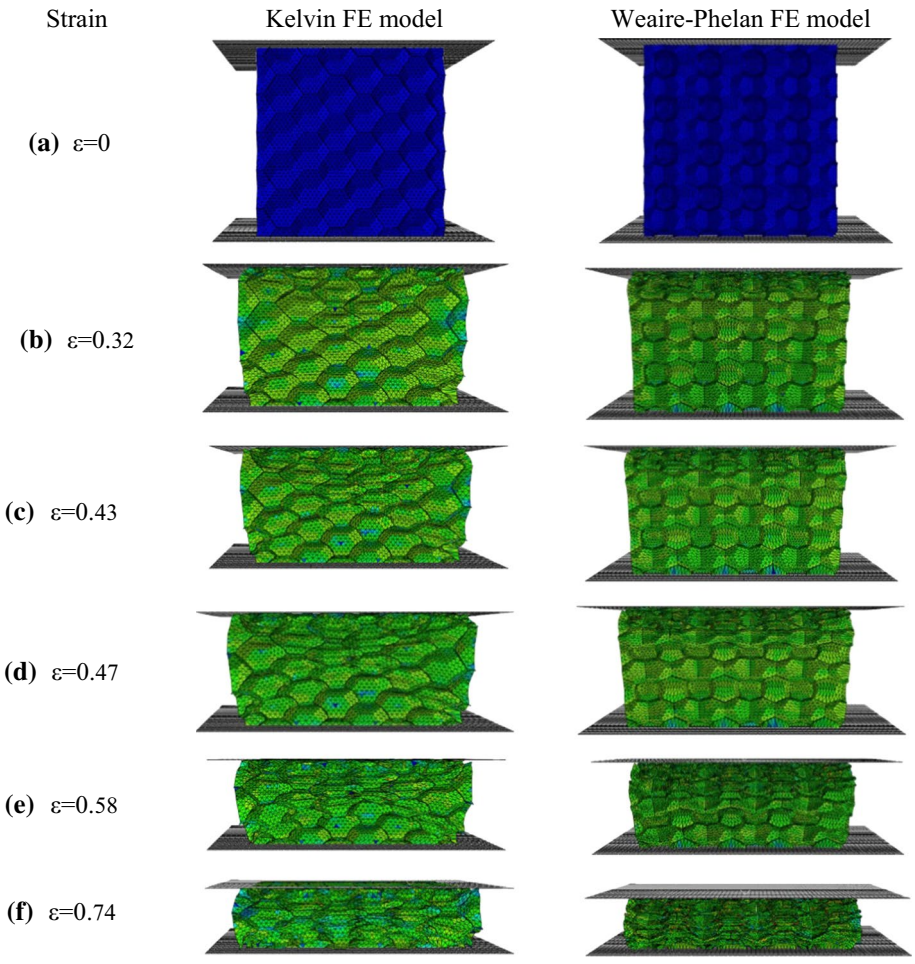

Fig. 10 Stress distribution in the Kelvin and Weaire–Phelan FE models at different strains: **a** $\varepsilon = 0$, **b** $\varepsilon = 0.32$, **c** $\varepsilon = 0.43$, **d** $\varepsilon = 0.47$, **e** $\varepsilon = 0.58$, and **f** $\varepsilon = 0.74$

The stress distribution in the Kelvin and Weaire–Phelan models at different global strains is compared in Fig. 10. As for the Kelvin model, at the global strain of 0.32 (Fig. 10b), the stress level in the inclined walls was around ~ 1.5 times higher than that in the horizontal walls. Moreover, by moving from the central region of the lattice structure towards its outer faces, the stress level increased by around 1.2 times. At the global strain of 0.43 and 0.47 (Fig. 10c,d), the stress was distributed relatively uniform throughout the whole structure. At the global strain of 0.58 (Fig. 10e), significant increase in the number of critical points appeared which had stress levels around two times the average stress level in the lattice structure. The number of critical points increased even further at the global strain level of 0.74 (Fig. 10f).

As for the Weaire–Phelan model, at the global strain of 0.32 (Fig. 10b), again, it was seen that the stress level increased slightly by moving from the central region of the lattice structure towards its sides, and therefore, the maximum stress level occured at the external faces of the lattice structure. According to the obtained stress contours, it was found out that the vertical walls experience stress levels ~ 1.1 times of the stress level in the horizontal walls. At the global strain of 0.43 and 0.47 (Fig. 10c,d), the vertical and horizontal walls experienced similar stress distributions. At the global strain of 0.58 (Fig. 10e), the stress distribution in the lattice structure was still relatively uniform, even though some critical points with high stress levels started showing up. By increasing the global strain to 0.74 (Fig. 10f), the number of critical points increased even further.

The stress distribution in the Weaire–Phelan model is, in general, more uniform as compared to that in Kelvin model (Fig. 10). This can be attributed to the Weaire–Phelan's more complex geometry (the presence of walls of more types, sizes, and orientations) which distributes the stress more uniformly.

4 Conclusion

In this study, quasi-static compression tests were conducted on aluminum foams. Kelvin and Weaire–Phelan FE models were constructed to evaluate which unit cell can better mimic the performance of metal closed-cell foams. The results indicated that:

1. First and foremost, both the numerical models are capable of predicating the behavior of metal closed-cell foams. Comparing the Kelvin and Weaire–Phelan FE models demonstrates that the Weaire–Phelan model better reconstructs the deformation of manufactured specimens. On the contrary, as compared to the Weaire–Phelan model, the mechanical properties obtained from the Kelvin model is in general slightly closer to the experimental results. It must be noted that the curves obtained from both the FE model types are very close to one another.
2. Due to the complexity of Weaire–Phelan unit cell as compared to Kelvin unit cell, the computational cost of solving a Weaire–Phelan model by FE code is less as compared to a Kelvin model. Moreover, as compared to the Kelvin model, the deformation of the Weaire–Phelan model during the compression was more similar to the experimental tests.
3. As the foam density increases, the densification strain decreases, while all other mechanical properties (elastic modulus, yield stress, plateau stress, and energy absorption capacity) increase.

4. The experimental densification strain is, in general, smaller than the numerical counterparts. This is due to the fact that during the plateau regime, several small particles are detached from the specimen and gradually fill in the internal pores of the foam. This detachment of small particles and filling of the pores are not, however, modelled in the numerical models. In lower densities, this difference in experimental/numerical densification strains becomes much smaller as the pore filling becomes of much less importance in foam behavior under compression.

Supplementary Information The online version contains supplementary material available at https://doi.org/10.1007/s11242-021-01729-5.

Funding This research received no funding.

Data Availability Data available on request from the corresponding author.

Code Availability The codes are available from the corresponding author on reasonable request.

Declarations

Conflict of interest The authors declare no conflict of interest.

Ethical Approval Not applicable.

References

Abdullahi, H.S., Liang, Y., Gao, S.: Predicting the elastic properties of closed-cell aluminum foams: a mesoscopic geometric modeling approach. SN Appl. Sci. **1**(4), 380 (2019)
Andrews, E., Gioux, G., Onck, P., Gibson, L.: Size effects in ductile cellular solids. Part II: experimental results. Int. J. Mech. Sci. **43**(3), 701–713 (2001)
Baillis, D., Coquard, R., Cunsolo, S.: Effective conductivity of Voronoi's closed-and open-cell foams: analytical laws and numerical results. J. Mater. Sci. **52**(19), 11146–11167 (2017)
Baillis, D., Coquard, R., Radiative and conductive thermal properties of foams. Cellular and Porous Materials: Thermal Properties Simulation and Prediction, p. 343–384, (2008)
Banhart, J.: Manufacture, characterisation and application of cellular metals and metal foams. Prog. Mater Sci. **46**(6), 559–632 (2001)
Buffel, B., Desplentere, F., Bracke, K., Verpoest, I.: Modelling open cell-foams based on the Weaire-Phelan unit cell with a minimal surface energy approach. Int. J. Solids Struct. **51**(19–20), 3461–3470 (2014)
Chen, Y., Das, R., Battley, M., EFFECTS OF CELL SIZE AND CELL WALL THICKNESS VARIATIONS ON THE STRENGTH OF CLOSED-CELL FOAMS USING LAGUERRE TESSELLATION
Czekanski, A., Attia, M., Meguid, S., Elbestawi, M.: On the use of a new cell to model geometric asymmetry of metallic foams. Finite Elem. Anal. Des. **41**(13), 1327–1340 (2005)
De Giorgi, M., Carofalo, A., Dattoma, V., Nobile, R., Palano, F.: Aluminium foams structural modelling. Comput. Struct. **88**(1–2), 25–35 (2010)
Diebels, S., Geringer, A.: Micromechanical and macromechanical modelling of foams: identification of Cosserat parameters. ZAMM-J. Appl. Math. Mech. **94**(5), 414–420 (2014)
Duarte, I., Vesenjak, M., Krstulović-Opara, L.: Compressive behaviour of unconstrained and constrained integral-skin closed-cell aluminium foam. Compos. Struct. **154**, 231–238 (2016)
Fang, Q., Zhang, J., Zhang, Y., Wu, H., Gong, Z.: A 3D mesoscopic model for the closed-cell metallic foams subjected to static and dynamic loadings. Int. J. Impact Eng **82**, 103–112 (2015)
Ghazi, A., Berke, P., Kamel, K.E.M., Sonon, B., Tiago, C., Massart, T.: Multiscale computational modelling of closed cell metallic foams with detailed microstructural morphological control. Int. J. Eng. Sci. **143**, 92–114 (2019)

Gibson, L.J., Ashby, M.F.: Cellular Solids: Structure and Properties. Cambridge University Press, Cambridge (1999)
Glicksman, L.R., Lanciani, A.J., Method and apparatus for improving the insulating properties of closed cell foam. 1991, Google Patents
Glicksman, L.R., Torpey, M.: Factors governing heat transfer through closed cell foam insulation. J. Therm. Insul. **12**(4), 257–269 (1989)
Grenestedt, J.L., Bassinet, F.: Influence of cell wall thickness variations on elastic stiffness of closed-cell cellular solids. Int. J. Mech. Sci. **42**(7), 1327–1338 (2000)
Hall, I.W., Güden, M., Yu, C.-J., Crushing of aluminum closed cell foams: density and strain rate effects. 2000
Han, F., Zhu, Z., Gao, J.: Compressive deformation and energy absorbing characteristic of foamed aluminum. Metall. Mater. Trans. A **29**(10), 2497–2502 (1998)
Hangai, Y., Minh, N.N., Morita, T., Suzuki, R., Matsubara, M., Koyama, S.: Cutting process for aluminum foam fabricated by sintering and dissolution process. Adv. Powder Technol. **28**(5), 1426–1429 (2017)
Hasan, M.: An improved model for FE modeling and simulation of closed cell Al-alloy foams. Adv. Mater. Sci. Eng. **2010**, 1–12 (2010)
Hedayati, R., Sadighi, M.: Effect of using an inner plate between two faces of a sandwich structure in resistance to bird-strike impact. J. Aerosp. Eng. **29**(1), 04015020 (2016)
Hedayati, R., Ziaei-Rad, S.: Foam-core effect on the integrity of tailplane leading edge during bird-strike event. J. Aircr. **48**(6), 2080–2089 (2011)
Hedayati, R., Hosseini-Toudeshky, H., Sadighi, M., Mohammadi-Aghdam, M., Zadpoor, A.: Multi-scale modeling of fatigue crack propagation in additively manufactured porous biomaterials. Int. J. Fatigue **113**, 416–427 (2018b)
Hedayati, R., Sadighi, M.: Low-velocity impact behaviour of open-cell foams. J. Theo. Appl. Mech. **56**, 939 (2018)
Hedayati, R., Ahmadi, S., Lietaert, K., Tümer, N., Li, Y., Amin Yavari, S., Zadpoor, A.: Fatigue and quasi-static mechanical behavior of bio-degradable porous biomaterials based on magnesium alloys. J. Biomed. Mater. Res. Part A **106**(7), 1798–1811 (2018)
Hedayati, R., Lakshmanan, S.: Pneumatically-actuated acoustic metamaterials based on Helmholtz resonators. Materials **13**(6), 1456 (2020). https://doi.org/10.3390/ma13061456
Hedayati, R., Salami, S.J., Li, Y., Sadighi, M., Zadpoor, A.: Semianalytical geometry-property relationships for some generalized classes of pentamodelike additively manufactured mechanical metamaterials. Phys. Rev. Appl. **11**(3), 034057 (2019)
Hedayati, R., Rubio Carpio, A., Luesutthiviboon, S., Ragni, D., Avallone, F., Casalino, D., van der Zwaag, S.: Role of polymeric coating on metallic foams to control the aeroacoustic noise reduction of airfoils with permeable trailing edges. Materials, **12**(7), 1087 (2019)
Heidari, M., Yan, J.: Material removal mechanism and surface integrity in ultraprecision cutting of porous titanium. Precis. Eng. **52**, 356–369 (2018)
Hu, Y., Fang, Q.-Z., Yu, H., Hu, Q.: Numerical simulation on thermal properties of closed-cell metal foams with different cell size distributions and cell shapes. Mater. Today Commun. **24**, 100968 (2020)
ISO, I., Mechanical testing of metals—ductility testing—compression test for porous and cellular metals*, 2011.* Google Scholar, 2011
Jang, W.-Y., Hsieh, W.-Y., Miao, C.-C., Yen, Y.-C.: Microstructure and mechanical properties of ALPORAS closed-cell aluminium foam. Mater. Charact. **107**, 228–238 (2015)
Kader, M., Hazell, P., Brown, A., Tahtali, M., Ahmed, S., Escobedo, J., Saadatfar, M.: Novel design of closed-cell foam structures for property enhancement. Addit. Manuf. **31**, 100976 (2020)
Kader, M., Brown, A., Hazell, P., Robins, V., Escobedo, J., Saadatfar, M.: Geometrical and topological evolution of a closed-cell aluminium foam subject to drop-weight impact: an X-ray tomography study. Int. J. Impact Eng. **139**, 103510 (2020)
Kadkhodapour, J., Raeisi, S.: Micro–macro investigation of deformation and failure in closed-cell aluminum foams. Comput. Mater. Sci. **83**, 137–148 (2014)
Karaji, Z.G., Hedayati, R., Pouran, B., Apachitei, I., Zadpoor, A.A.: Effects of plasma electrolytic oxidation process on the mechanical properties of additively manufactured porous biomaterials. Mater. Sci. Eng. C **76**, 406–416 (2017)
Koloushani, M., Hedayati, R., Sadighi, M., Mohammadi-Aghdam, M.: CT-based micro-mechanical approach to predict response of closed-cell porous biomaterials to low-velocity impact. J. Imaging **4**(3), 49 (2018)
Li, Z., Zhang, J., Fan, J., Wang, Z., Zhao, L.: On crushing response of the three-dimensional closed-cell foam based on Voronoi model. Mech. Mater. **68**, 85–94 (2014)

Li, Z.-B., Li, X.-Y., Zheng, Y.-X.: Biaxial mechanical behavior of closed-cell aluminum foam under combined shear—compression loading. Trans. Nonferr. Metals Soc. China **30**(1), 41–50 (2020)
Liu, X., Zhang, J., Fang, Q., Wu, H., Zhang, Y.: Response of closed-cell aluminum foams under static and impact loading: experimental and mesoscopic numerical analysis. Int. J. Impact Eng **110**, 382–394 (2017)
Liu, Y., Zhou, W., Chu, X., Liu, S., Hui, K.S.: Feasibility investigation of direct laser cutting process of metal foam with high pore density. Int. J. Adv. Manuf. Technol. **96**(5–8), 2803–2814 (2018)
Liu, Y., Zhou, W., Li, X., Chu, X., Cai, S.: Experimental investigations on cutting force and temperature in milling process of copper foam with high porosity. Int. J. Adv. Manuf. Technol. **108**, 759–767 (2020)
Liu, C., Zhang, Y., MODELLING MECHANICAL BEHAVIOR OF ALUMINIUM FOAM UNDER COMPRESSIVE LOADING USING REPRESENTATIVE VOLUME ELEMENT METHOD, (2013)
Marvi-Mashhadi, M., Lopes, C., J. LLorca,: Effect of anisotropy on the mechanical properties of polyurethane foams: an experimental and numerical study. Mech. Mater. **124**, 143–154 (2018)
Marvi-Mashhadi, M., Lopes, C., Lorca, J.L.: Modelling of the mechanical behavior of polyurethane foams by means of micromechanical characterization and computational homogenization. Int. J. Solids Struct. **146**, 154–166 (2018)
Marvi-Mashhadi, M., Lopes, C., J. LLorca,: High fidelity simulation of the mechanical behavior of closed-cell polyurethane foams. J. Mech. Phys. Solids **135**, 103814 (2020)
Meng, K., Chai, C., Sun, Y., Wang, W., Wang, Q., Li, Q.: Cutting-induced end surface effect on compressive behaviour of aluminium foams. Eur. J. Mech.-A/Solids **75**, 410–418 (2019)
Mills, N., Stämpfli, R., Marone, F., Brühwiler, P.: Finite element micromechanics model of impact compression of closed-cell polymer foams. Int. J. Solids Struct. **46**(3–4), 677–697 (2009)
Mohammadi Nasrabadi, A., Hedayati, R., Sadighi, M.: Numerical and experimental study of the mechanical response of aluminum foams under compressive loading using CT data. J. Theo. Appl. Mech. **54**, 1357 (2016)
Motz, C., Pippan, R.: Deformation behaviour of closed-cell aluminium foams in tension. Acta Mater. **49**(13), 2463–2470 (2001)
Movahedi, N., Mirbagheri, S., Hoseini, S.: Effect of foaming temperature on the mechanical properties of produced closed-cell A356Aluminum foams with melting method. Met. Mater. Int. **20**(4), 757–763 (2014)
Nammi, S., Myler, P., Edwards, G.: Finite element analysis of closed-cell aluminium foam under quasi-static loading. Mater. Des. **31**(2), 712–722 (2010)
Novak, N., Vesenjak, M., Duarte, I., Tanaka, S., Hokamoto, K., Krstulović-Opara, L., Guo, B., Chen, P., Ren, Z.: Compressive behaviour of closed-cell aluminium foam at different strain rates. Materials **12**(24), 4108 (2019)
Opiela, K.C., Zieliński, T.G., Dvorák, T., Kudela, S., Jr.: Perforated closed-cell aluminium foam for acoustic absorption. Appl. Acoust. **174**, 107706 (2021)
Pabst, W., Uhlířová, T., Gregorová, E., Wiegmann, A.: Young's modulus and thermal conductivity of closed-cell, open-cell and inverse ceramic foams–model-based predictions, cross-property predictions and numerical calculations. J. Eur. Ceram. Soc. **38**(6), 2570–2578 (2018)
Rajendran, R., Moorthi, A., Basu, S.: Numerical simulation of drop weight impact behaviour of closed cell aluminium foam. Mater. Des. **30**(8), 2823–2830 (2009)
Ramamurty, U., Paul, A.: Variability in mechanical properties of a metal foam. Acta Mater. **52**(4), 869–876 (2004)
Razboršek, B., Gotlih, J., Karner, T., Ficko, M., Razboršek, B., Ficko, J.G.T.K.M.: The influence of machining parameters on the surface porosity of a closed-cell aluminium foam. Stroj. Vestn.–J. Mech. Eng. **66**, 29–37 (2019)
Roberts, A.P., Garboczi, E.J.: Elastic moduli of model random three-dimensional closed-cell cellular solids. Acta Mater. **49**(2), 189–197 (2001)
Santosa, S., Wierzbicki, T.: On the modeling of crush behavior of a closed-cell aluminum foam structure. J. Mech. Phys. Solids **46**(4), 645–669 (1998)
Shi, X., Liu, S., Nie, H., Lu, G., Li, Y.: Study of cell irregularity effects on the compression of closed-cell foams. Int. J. Mech. Sci. **135**, 215–225 (2018)
Simone, A., Gibson, L.: Effects of solid distribution on the stiffness and strength of metallic foams. Acta Mater. **46**(6), 2139–2150 (1998)
Sun, Y., Amirrasouli, B., Razavi, S.B., Li, Q., Lowe, T., Withers, P.: The variation in elastic modulus throughout the compression of foam materials. Acta Mater. **110**, 161–174 (2016)
Thomson, W.: On the division of space with minimum partitional area. Acta Math. **11**, 121–134 (1887)
Torkestani, A., Sadighi, M., Hedayati, R.: Effect of material type, stacking sequence and impact location on the pedestrian head injury in collisions. Thin-Walled Struct. **97**, 130–139 (2015)

Tzeng, S.-C., Ma, W.-P.: A novel approach to manufacturing and experimental investigation of closed-cell Al foams. Int. J. Adv. Manuf. Technol. **28**(11–12), 1122–1128 (2006)
Ulbin, M., Vesenjak, M., Borovinšek, M., Duarte, I., Higa, Y., Shimojima, K., Ren, Z.: Detailed analysis of closed-cell aluminum alloy foam internal structure changes during compressive deformation. Adv. Eng. Mater. **20**(8), 1800164 (2018)
Ulbin, M., Glodež, S., Vesenjak, M., Duarte, I., Podgornik, B., Ren, Z., Kramberger, J.: Low cycle fatigue behaviour of closed-cell aluminium foam. Mech. Mater. **133**, 165–173 (2019)
Ulbin, M., Kramberger, J., Glodež, S.: Low-cycle fatigue analysis of closed-cell aluminium foam using a homogenised material model. Mech. Mater. **145**, 103397 (2020)
Vengatachalam, B., Poh, L., Liu, Z., Qin, Q., Swaddiwudhipong, S.: Three dimensional modelling of closed-cell aluminium foams with predictive macroscopic behaviour. Mech. Mater. **136**, 103067 (2019)
Wang, P., Xu, S., Li, Z., Yang, J., Zhang, C., Zheng, H., Hu, S.: Experimental investigation on the strain-rate effect and inertia effect of closed-cell aluminum foam subjected to dynamic loading. Mater. Sci. Eng., A **620**, 253–261 (2015)
Wang, H., Liu, B., Kang, Y.-X., Qin, Q.-H.: Analysing effective thermal conductivity of 2D closed-cell foam based on shrunk Voronoi tessellations. Arch. Mech. **69**(6), 451–470 (2017)
Weaire, D., Phelan, R.: A counter-example to Kelvin's conjecture on minimal surfaces. Philos. Mag. Lett. **69**(2), 107–110 (1994)
Yilbas, B., Akhtar, S., Keles, O.: Laser hole cutting in aluminum foam: influence of hole diameter on thermal stress. Opt. Lasers Eng. **51**(1), 23–29 (2013)
Yilbas, B.S., Akhtar, S., Keles, O.: Laser cutting of triangular blanks from thick aluminum foam plate: thermal stress analysis and morphology. Appl. Therm. Eng. **62**(1), 28–36 (2014)
Yilbas, B., Akhtar, S., Keles, O.: Laser cutting of small diameter hole in aluminum foam. Int. J. Adv. Manuf. Technol. **79**(1–4), 101–111 (2015)
Zenkert, D., Burman, M.: Tension, compression and shear fatigue of a closed cell polymer foam. Compos. Sci. Technol. **69**(6), 785–792 (2009)
Zhu, W., Blal, N., Cunsolo, S., Baillis, D., Michaud, P.-M.: Effective elastic behavior of irregular closed-cell foams. Materials **11**(11), 2100 (2018)